

# Integrated Optical Ti:Er:LiNbO<sub>3</sub> Soliton Source

H. Suche, *Associate Member, IEEE*, A. Greiner, W. Qiu, R. Wessel, and Wolfgang Sohler, *Associate Member, IEEE*

(Invited Paper)

**Abstract**—Efficient diode-pumped and harmonically mode-locked operation of a fully packaged Ti:Er:LiNbO<sub>3</sub> waveguide laser at 1562-nm (TE) and 1575-nm (TM) wavelength has been demonstrated. The mode-locked pulses have been characterized in terms of time-bandwidth product, fine tuning, and stability. Noise suppression of 42 dB at the relaxation oscillation frequency has been achieved by feedback-controlled pumping. An external amplitude modulator has been used for encoding of the mode-locked pulse train with different bit sequences. Bit error rates of  $10^{-10}$  for a 1-0-1-0-bit sequence has been observed for more than half an hour.

**Index Terms**—Diffusion processes, Er-doping, harmonic mode locking, integrated optics, lithium niobate, optical solitons.

## I. INTRODUCTION

MODE-LOCKING is a versatile means to generate pulse trains of high repetition rate and peak power. Therefore, a mode-locked laser emitting in the third telecommunication window is regarded as a very promising source for high-bit-rate soliton-type data transmission. Integrated optical versions of such a mode-locked source are rugged and have a high potential for miniaturization. Moreover, sources in electrooptic materials allow the monolithic integration of an active mode-locker [1] and in this way the required synchronization to a system clock for digital data transmission.

Er-doped LiNbO<sub>3</sub> is an attractive material for the realization of such a mode-locked source. It has excellent electrooptic properties and allows the incorporation of Er up to the solid solubility limit without fluorescence quenching and the fabrication of high-quality Er-doped waveguides [2]. Using a monolithically integrated intracavity phase modulator as mode-locker (FM-type mode-locking) and a broad-band Fabry-Perot waveguide cavity, fundamental and harmonic mode-locking [3], [4], [5] have already been demonstrated. With harmonic mode-locking high pulse repetition rates can be achieved with long laser cavities leading especially for Er-doped lasers to an improved pump absorption and laser output efficiency, respectively.

Using this concept, an efficient (14% slope efficiency) diode-pumped and fully packaged harmonically mode-locked laser has been developed. In this paper, we report the fabrication of this laser, its properties during CW and harmonically mode-locked operation and bit-error-rate (BER) investigations

Manuscript received March 27, 1997. This work was supported by the European Union within the ACTS Project ESTHER (AC 063) and by the Heinz Nixdorf Institut, University of Paderborn, Germany.

The authors are with the Universität-GH Paderborn, Angewandte Physik, D-33098 Paderborn, Germany.

Publisher Item Identifier S 0018-9197(97)07092-9.

of soliton-type RZ data achieved by external encoding of the pulsed laser output. This laser will be tested in soliton communication experiments within the European ACTS Project ESTHER (AC063).

## II. LASER FABRICATION AND SETUP OF THE SOLITON SOURCE

In this section, the fabrication and properties of the different laser components and the pigtailling and packaging together with additional fiberoptic components are discussed.

### A. Laser Fabrication

Half (with respect to the X-direction) of the Z-cut (Y-propagation) LiNbO<sub>3</sub> substrate has been doped near the surface by indiffusion of a 28-nm-thick layer of vacuum-deposited Er at 1130 °C during 125 h. Subsequently, photolithographically defined 7- $\mu$ m-wide and 98-nm-thick Ti stripes have been indiffused at 1060 °C during 8 h to form the 66.5-mm-long waveguide channels. Attenuation figures of the undoped channels down to 0.02 dB/cm (TE) and 0.05 dB/cm (TM) have been measured at 1523-nm wavelength, respectively. In the doped waveguides, almost the same scattering losses can be estimated from the difference between the measured transmission and absorption. The FWHM figures of the near-field intensity distributions of the modes at 1556-nm wavelength are 6.3  $\mu$ m  $\times$  4.4  $\mu$ m (width  $\times$  depth; TE) and 4.6  $\mu$ m  $\times$  3.1  $\mu$ m (TM), respectively. Within experimental error, the intensity distributions are identical for doped and undoped channels.

To avoid excess losses of the TM mode, an 0.6- $\mu$ m-thick insulating SiO<sub>2</sub> buffer layer has been vacuum deposited onto the substrate surface prior to the electrode fabrication.

The electrode structure of the intracavity traveling-wave phase modulator (mode locker) is a symmetrical coplanar microstrip line (as indicated in Fig. 1) with a gap to hotline width ratio of 0.75, a hot line width of about 11  $\mu$ m, and a length of 15 mm. First, a thin electrode has been fabricated by photolithographic lift-off of a sandwich of 30-nm sputtered Ti and 120-nm sputtered Au. Subsequently, the Au structure was electroplated up to a thickness of 4.5  $\mu$ m using a cyanidic Au electrolyte.

To determine the halfwave voltage of the intracavity phase modulator, the Er-doped waveguide resonator has been operated as an electrooptical spectrum analyzer [6]. As a signal, the output of a DFB laser diode ( $\lambda = 1546$  nm) has been launched into the Er-doped waveguide cavity. A sawtooth voltage has been applied to the modulator electrodes and the voltage difference between two adjacent resonances of the cavity (which is equal to the halfwave voltage  $V_{\pi}$ ) has been

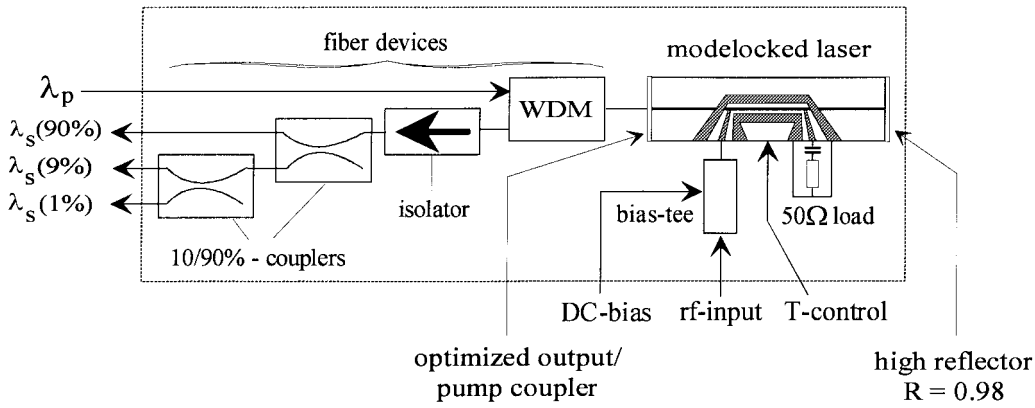


Fig. 1. Schematic structure of the pigtailed and packaged laser.

measured for both, TE and TM polarizations.  $V_{\pi}$  is 5.4 V for TM and 21.6 V for TE, respectively, due to the difference between the electrooptic coefficients and the field overlaps for TE and TM polarizations.

To drive the mode-locker, the radio frequency (RF) signal from a highly stable generator was boosted using a low-noise power amplifier and then fed via a bias tee to the traveling-wave electrodes of the intracavity phase modulator. The electrodes are terminated (ac) by a 50- $\Omega$  load (see Fig. 1).

The laser cavity is comprised of a high reflector on the rear side and a pump input coupler of optimized output coupling for the signal (see Fig. 1). Both mirrors consist of SiO<sub>2</sub>-TiO<sub>2</sub> layers directly deposited onto the polished waveguide endfaces using O<sub>2</sub><sup>+</sup> ion-assisted reactive evaporation. The rear mirror consists of 13 layers quarterwave at 765 nm leading to about 98% reflectivity at both pump and signal wavelengths. The output coupler consists of 14 layers quarterwave at 946 nm leading to a minimum reflectivity of about 7% at the pump wavelength ( $\lambda \approx 1480$  nm) and an output coupling of the signal of about 55% (see Fig. 2, test glass).

### B. Packaging

After characterization of the laser chip, the pump input side of the cavity was pigtailed with the common branch of a fiberoptic wavelength division demultiplexer (WDM) to allow coupling of a pigtailed pump laser diode and extraction of the laser output in backward direction (see Fig. 1). The WDM has standard (9/125  $\mu$ m) fiber pigtailed. Its signal branch has been optically isolated to prevent feedback-induced instabilities. The laser output is further split using two cascaded 10%/90% fiber optical power splitters for monitoring of the mode-locking stability, of the pulse peak power and to derive a control signal for feedback stabilization. FC receptacles are provided for the pump input, for the main laser output (90%), and for the two tap outputs (9%, 1%). The pigtailed laser has been mounted on a thermoelectrically controlled Cu heat sink allowing an accurate temperature stabilization ( $\pm 0.01$  K). All the components mentioned above are assembled in a housing which can be plugged together with other components into a common 19-in rack (see photograph of the rack in Fig. 3). From left to right in Fig. 3, the following plug-ins are shown: pump laser diode with built-in polarization

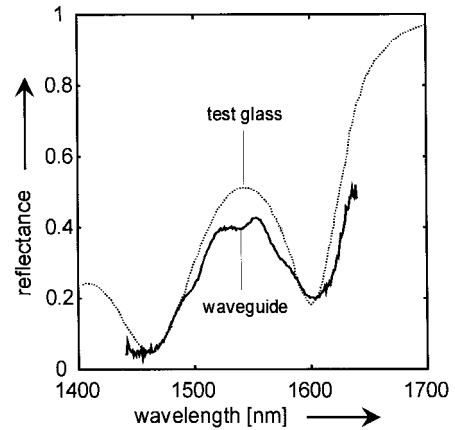


Fig. 2. Measured reflectance versus wavelength of the output coupler resp. pump coupler of the Ti:Er:LiNbO<sub>3</sub> waveguide laser cavity; solid graph: internal reflectance of the waveguide mode; dashed graph: reflectance of the test glass (coated together with the polished waveguide endface) at normal incidence.

controller, mode-locked Ti:Er:LiNbO<sub>3</sub> waveguide laser with FC receptacles for the pump input and the three outputs, SMA connectors for RF- and bias input, RF-booster amplifier to drive the modelocker, power supply, SHG generator to monitor the peak power of the mode-locked pulses, and pA meter to read out the SHG detector.

For bit-error-rate investigations, the 90% output port of the laser has been launched through a commercial Mach-Zehnder-type Ti:LiNbO<sub>3</sub> intensity modulator for data encoding. The modulator has a halfwave voltage  $V_{\pi}$  of 4.3 V (at 1 kHz) and an optical bandwidth ( $-3$  dB) of 5 GHz. A polarization controller has been used to adjust the input polarization state to TM for maximum extinction ratio (23 dB).

### III. SOURCE PROPERTIES

In this section, the properties of the laser during CW and during mode-locked operation are presented. First the power characteristics for CW operation and the properties of the mode-locked pulses in the time- and wavelength domain are shown. Then results of BER measurements after external data encoding are presented. Finally, the noise properties which determine the stability of launched solitons are discussed.



Fig. 3. Photograph of the rack-mounted, packaged soliton source (for more details see text).

#### A. Power Characteristics

To pump the Ti:Er:LiNbO<sub>3</sub> waveguide laser a high-power laser diode of about 1480-nm center wavelength and 12-nm spectral width has been used. The pump power was launched through the WDM into the mode-locked laser (see Fig. 1). Up to 140 mW of incident pump power were available at the common branch of the WDM. In Fig. 4, the CW power characteristics of the Er laser is shown for TM( $\pi$ )-polarized emission at 1575-nm and TE( $\sigma$ )-polarized emission at 1562-nm wavelength, respectively. The polarization and wavelength of the emission can be adjusted by the pump polarization. With  $\pi(\sigma)$ -polarized pumping, the Er laser emits at 1575(1562) nm  $\pi(\sigma)$ -polarized. Threshold pump power levels and slope efficiencies are 56 mW (65 mW) and 14.4% (13.2%) for  $\pi(\sigma)$ -polarized emission, respectively. Both slope efficiency and output power are more than an order of magnitude better than previously reported results [3], [4].

#### B. Pulse Properties

Mode-locking has been achieved by phase modulation (FM-type mode-locking) synchronously with different harmonics of the axial-mode frequency spacing of the laser cavity. Results are shown for the fifth harmonic as the corresponding pulse repetition frequency at about 5 GHz is of most interest for the ACTS project mentioned above. BER measurements have been carried out at the second harmonic due to actual limitations of the data rate of the available pattern generator.

To determine the polarization-dependent axial-mode frequency spacing of the waveguide cavity, the laser output in CW operation was detected and the Fourier component of the beat frequency of the axial eigenmodes was determined using an electronic spectrum analyzer. The mode spacing is

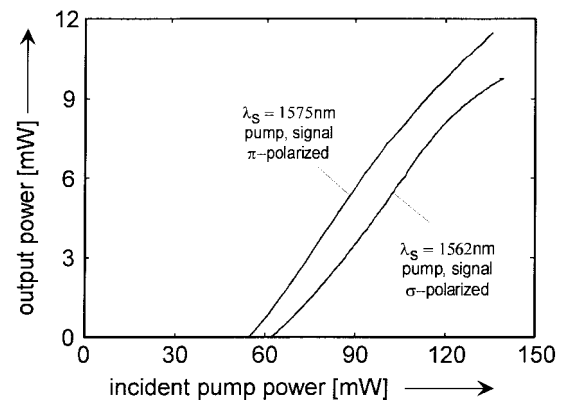


Fig. 4. Output power versus pump power incident at the common branch of the  $f/o$  WDM coupler (see Fig. 2) for both  $\pi$ - and  $\sigma$ -polarized emission. The polarization-dependent emission wavelengths are indicated.

994.3 MHz for TE and 1029.5 MHz for TM polarization. This method also provides a very precise determination of the mode effective indices.

In Fig. 5, the laser output pulses are shown in the wavelength- and time domain for the fifth harmonic (5.147 66 GHz) and  $\pi$ -polarized emission at 1575-nm wavelength for two different levels of the RF drive power. With 29 dBm of RF power, a pulsewidth of 7.4 ps (FWHM) has been determined by the deconvolution of the autocorrelation trace assuming a Gaussian pulse shape. Together with the spectral width of 0.77 nm, a time-bandwidth product of 0.68 results, indicating a slight frequency chirp of the pulses. Pulse peak power levels up to 310 mW have been achieved which are more than sufficient for soliton generation in dispersion-shifted fibers. For 16 dBm of RF power, the pulsewidth broadens to about

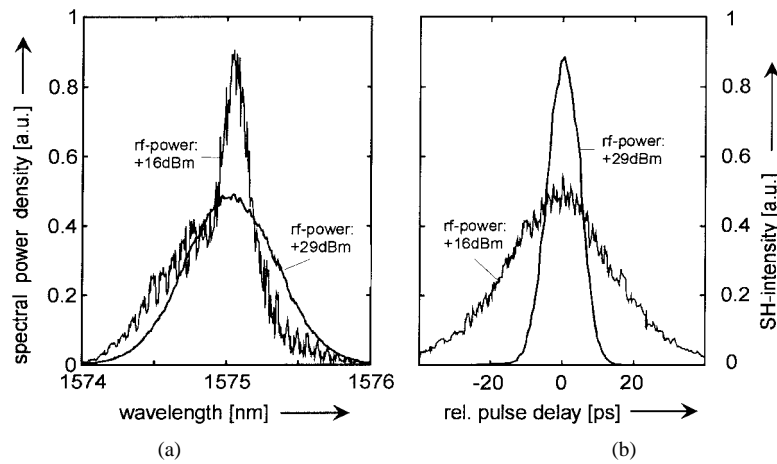


Fig. 5. (a) Spectral power density versus wavelength and (b) autocorrelation trace (SH intensity) as function of the relative pulse delay for mode-locking at the fifth harmonic (5.14766 GHz) in  $\pi$ -polarized emission ( $\lambda = 1575$  nm).

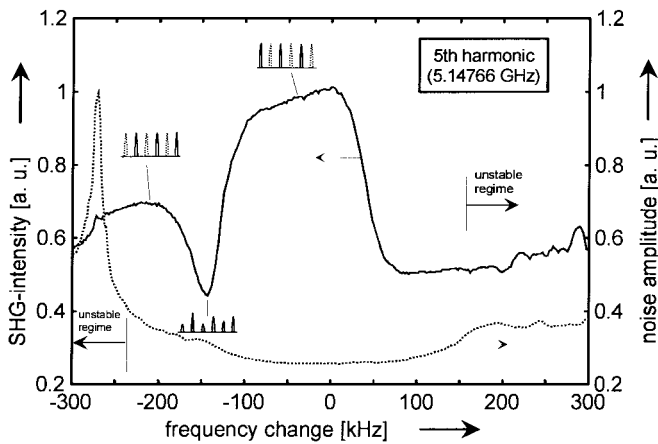


Fig. 6. Second harmonic intensity (upper solid graph, left ordinate) and low-frequency rms noise amplitude (lower dashed graph, right ordinate) for fifth harmonic mode-locking at 1575-nm wavelength,  $\pi$ -polarized, versus frequency deviation from the optimum locking condition (maximum pulse peak power).

21 ps and the spectral width can be estimated to 0.26 nm. However, the stability of the pulses is significantly deteriorated as can be seen from the noise on both the correlation trace and the spectrum in Fig. 5. During these measurements, controlled pumping of the mode-locked laser has been used to reduce the low frequency noise (see next subsection for more details).

With  $\sigma$ -polarized emission at 1562 nm wavelength fifth harmonic mode-locking has been obtained at 4.971 33 GHz. Time-bandwidth products down to 0.45 have been achieved.

For FM mode-locking, it is well known from theory [7] that two interleaved pulse trains can exist which are synchronized with the positive and negative extremes of the phase modulation, respectively. Due to material dispersion the frequency degeneracy for the excitation of these trains is removed [7]. Using a small angle-tuned optical second harmonic (SH) generator, we have monitored the peak power of the mode-locked pulses as function of the fine tuning of the RF-drive frequency for the mode-locker. Simultaneously, the low-frequency (bandwidth: 20 Hz–300 kHz) rms noise amplitude of the average laser output power has been recorded and the timing of the pulses monitored relative to the RF-

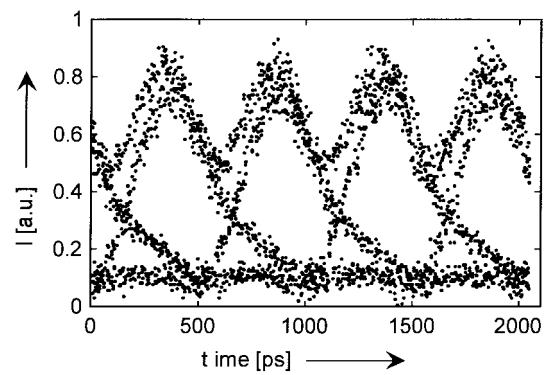


Fig. 7. Eye diagram of a  $2^{23} - 1$  PRBS achieved by external modulation (encoding) of the waveguide laser output during second harmonic mode-locking; emission wavelength and polarization are 1562 nm and  $\sigma$ , respectively.

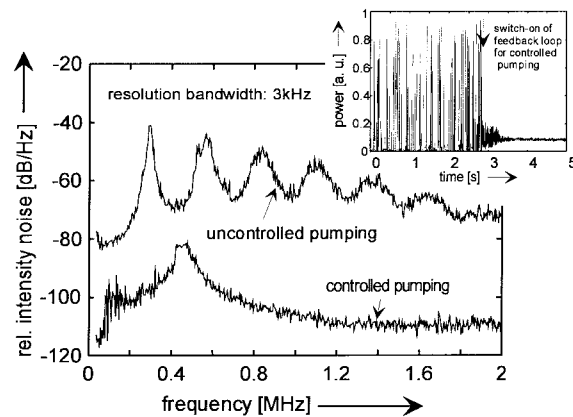


Fig. 8. RIN versus frequency of the laser during fifth harmonic mode-locking at 1575-nm wavelength,  $\pi$ -polarized, for uncontrolled and controlled pumping; inset: transient behavior of the laser output power upon closing of the feedback loop for controlled pumping.

drive signal using a fast (15-GHz optical bandwidth) InGaAs PIN photodiode and a sampling scope. The result of such a measurement for  $\pi$ -polarized emission at 1575 nm is shown in Fig. 6. There is a low noise regime related to a fairly stable operation of either of the two pulse trains where the SH generator has a strong signal. In between, both trains coexist and compete, leading to a reduced peak power of the individual pulses. As a

result, the SH signal has a strong dip in this range. Obviously, the tolerance in the RF drive frequency for stable high-peak-power mode-locking at the fifth harmonic is about 100 kHz.

To assess the stability of the source for RZ-type soliton data transmission, we have launched the main output of the mode-locked laser through a Mach-Zehnder-type LiNbO<sub>3</sub> modulator and have driven the modulator with different NRZ data patterns for digital encoding. The encoded output has been detected, amplified by 32 dB, and investigated with a commercial BER detector. In addition, the eye pattern of the soliton transmitter has been observed. In Fig. 7, an example of an eye diagram for second harmonic mode-locking of the 1562-nm emission of the laser is shown for a pseudorandom bit sequence (PRBS) of  $2^{23} - 1$ . Due to the limitations in the bandwidth of our preamplifier (50-MHz lower frequency limit), low error rates for long PRBS's cannot be achieved. Therefore, we tested the pulse stability using a 1-0-1-0-bit sequence. With this sequence, BER's of about  $10^{-10}$  have been achieved for gating times in excess of half an hour. To achieve this result, the RF-drive frequency had to be detuned about 500 kHz from the frequency of minimum time-bandwidth product of the mode-locked pulses.

An upgrade of the BER setup will allow the investigation of the transmitter up to tenth harmonic mode-locking in the near future.

### C. Laser Noise

In mode-locked laser operation, two main contributions to the laser noise can be distinguished: low-frequency amplitude noise mainly due to relaxation oscillations and spiking, respectively, and for FM mode-locking the competition of the two interleaved pulse trains (as discussed above); and high-frequency noise due to the competition of supermodes for harmonic mode-locking.

To suppress relaxation spiking of the laser during mode-locking, 9% of the laser output were detected and the detector signal fed to a specially designed electronic control circuit. This circuit generates and superimposes a correction component to the injection current of the pump laser diode to suppress relaxation oscillations. Up to 42-dB reduction of the spectral power density at the dominant peak of the noise spectrum has been achieved, leading to a relative intensity noise (RIN) of  $-82.3$  dB/Hz at the residual relaxation oscillation peak around 450 kHz for 3.5 dBm of dc electrical power (detector signal into  $50 \Omega$  corresponding to 6.7 mW of average optical power) (see Fig. 8). At frequencies above 100 MHz, the laser output is almost shot noise limited. Only at frequencies corresponding to integers of the axial mode spacing can significant peaks in the electronic spectrum be observed. In addition to the Fourier component at the mode-locking frequency, further components have been observed at other harmonics of the axial mode frequency spacing as a result of supermode competition (for  $N$ th harmonic mode-locking  $N$  combs of axial modes (so-called supermodes) can exist which are offset one axial mode spacing against each other but generate pulse trains of the same period).

In the literature, a number of methods have been reported for the suppression of supermode competition noise during harmonic mode-locking (see, e.g., [8]–[10]).

We are currently investigating low-frequency intracavity phase modulation as a means to suppress supermode competition. Up to 8-dB suppression of the beat component at the axial mode frequency spacing has already been observed for  $\pi$ -polarized emission at 1575-nm wavelength.

## IV. CONCLUSION

We have fabricated and investigated an efficient harmonically mode-locked Ti:Er:LiNbO<sub>3</sub> soliton source. Its power characteristics, pulse properties, noise, and BER after encoding have been studied. By feedback-controlled pumping, the low-frequency RIN of the laser could be reduced by 42 dB. BER's down to  $10^{-10}$  have been observed for a 1-0-1-0-bit sequence. Error-free launching of real data (broad Fourier spectrum) for long-haul soliton transmission at 10 Gbit/s still requires a better suppression of supermode competition.

## ACKNOWLEDGMENT

The authors thank Prof. Noé for borrowing the BER setup.

## REFERENCES

- [1] E. Lallier, J. P. Pocholle, M. Papuchon, M. de Micheli, M. J. Li, Q. He, and C. Grezes-Besset, "Integrated Nd:MgO:LiNbO<sub>3</sub> FM mode locked-waveguide laser," *Electron. Lett.*, vol. 27, no. 11, pp. 936–937, 1991.
- [2] I. Baumann, R. Brinkmann, M. Dinand, W. Sohler, L. Beckers, Ch. Buchal, M. Fleuster, H. Holzbrecher, H. Paulus, K.-H. Müller, Th. Gog, G. Materlik, O. Witte, H. Stolz, and W. von der Osten, "Erbium incorporation in LiNbO<sub>3</sub> by diffusion-doping," *Appl. Phys. A*, vol. 64, pp. 33–44, 1997.
- [3] H. Suche, I. Baumann, D. Hiller, and W. Sohler, "Modelocked Er:Ti:LiNbO<sub>3</sub>-waveguide laser," *Electron. Lett.*, vol. 29, no. 12, pp. 1111–1112, 1993.
- [4] H. Suche, R. Wessel, S. Westenhöfer, W. Sohler, S. Bosso, C. Carmanini, and R. Corsini, "Harmonically modelocked Ti:Er:LiNbO<sub>3</sub>-waveguide laser," *Opt. Lett.*, vol. 20, no. 6, pp. 596–598, 1995.
- [5] H. Suche, A. Greiner, W. Qiu, R. Wessel, and W. Sohler, "Efficient diode pumped, harmonically modelocked Ti:Er:LiNbO<sub>3</sub>-waveguide laser for soliton transmission," in *8th Europ. Conf. Integrated Optics, ECIO'97*, Stockholm, Sweden, 1997, paper EThA3.
- [6] H. Suche, D. Hiller, I. Baumann, and W. Sohler, "Integrated optical spectrum analyzer with internal gain," *IEEE Photon. Technol. Lett.*, vol. 7, pp. 505–507, 1995.
- [7] D. J. Kuizenga and A. E. Siegman, "FM and AM mode locking of the homogeneous laser—Part I: Theory," *IEEE J. Quantum Electron.*, vol. QE-6, pp. 694–708, 1970.
- [8] X. Shan and D. M. Spirit, "Novel method to suppress noise in harmonically modelocked erbium fiber lasers," *Electron. Lett.*, vol. 29, no. 11, pp. 979–981, 1993.
- [9] P. Singh, T. Tazaki, K. Ikeda, M. Mori, T. Goto, and A. Miyauchi, "Mode-locking of fiber ring lasers with a coherent-phase relationship among axial mode groups," *Opt. Laser Technol.*, vol. 27, no. 4, pp. 275–277, 1995.
- [10] M. Nakazawa, K. Tamura, and E. Yoshida, "Supermode noise suppression in a harmonically modelocked fiber laser by selfphase modulation and spectral filtering," *Electron. Lett.*, vol. 32, no. 5, pp. 461–463, 1996.

**H. Suche** (A'95), photograph and biography not available at the time of publication.

**A. Greiner**, photograph and biography not available at the time of publication.

**W. Qiu**, photograph and biography not available at the time of publication.

**R. Wessel**, photograph and biography not available at the time of publication.

**Wolfgang Sohler** (A'88), photograph and biography not available at the time of publication.